Journal of the Optical Society of Korea, Vol. 7, No. 3, September 2003, pp. 160-165

Micromachining of Cr Thin Film and Glass Using an Ultrashort Pulsed Laser

Ji Yeon Choi*, Jae Gu Kim, Bo Sung Shin, and Kyung Hyun Whang

Nano process group, Korea Institute of Machinery and Materials, Daejeon 305-343, KOREA

(Received June 30, 2002)

Materials processing by ultrashort pulsed laser is actively being applied to micromachining technology due to its advantages with regard to non-thermal machining. In this study, materials processing with ultrashort pulses was studied by using the high repetition rate of a 800 nm Ti:sapphire regenerative amplifier. This revealed that the highly precise micromachining of metallic thin film and bulk glass with a minimal heat affected zone (HAZ) could be obtained by using near damage threshold energy. Grooves with diffraction limited sub-micrometer width were obtained with widths of 620 nm on Cr thin film and 800 nm on a soda-lime glass substrate. The machined patterns were investigated through SEM images. We also phenomenologically examined the influence of variations of parameters and proposed the optimal process conditions for microfabrication.

OCIS codes : 320.0320, 350.3850, 270.4180.

I. INTRODUCTION

Laser manufacturing has evolved rapidly since the development of the laser in the 1960s. Laser based manufacturing technologies, such as welding, cutting, and drilling, appeared in the early history of the laser and have been actively applied to operations in various fields such as surgical operations and the restoration of cultural assets. The benefit of employing lasers in such various fields is that a laser, through a contactless method, can machine material of small size without any damage in a short time by rapidly irradiating a great deal of energy into a narrow area. Therefore, precise micromachining is possible with high peak power and short pulse duration. Because the sizes of devices today are becoming much smaller with technological advances, laser machining with ultrashort pulses has considerable meaning as a strong tool for micro-devices. Consequently, numerous researchers have studied micro-manufacturing technology using ultrashort pulse lasers.

Ultrashort pulse laser machining has been developed since the introduction of the CPA method in the mid-1980s [1]. Currently, ultrashort pulse laser micromachining technologies are being developed as a universal tool to approach micromachining from a micrometer to sub-micrometer range with flexibility and high precision. But theoretical analysis of ablation by ultrashort pulse has yet to be completed. For an ultrashort pulse duration regime, it is well known that nonthermal photochemical ablation is dominant, because laser pulse duration is shorter than the electron-lattice interaction time constant [2,3]. This is a key aspect for nonthermal fabrication of micro-devices. Various industrial applications have been demonstrated by using Ti:sapphire pulse with sub-ps duration, such as fuel injection nozzles, mask repair, and optical device fabrication [4–7]. In the near future these applications will be suitable for industrial mass-product machining environments. Therefore it is of potential benefit to study materials processing using ultrashort pulses for industrial manufacturing applications.

In this paper, we show some phenomenological characteristics of interactions between ultrashort pulse and materials, particularly Cr thin film and soda-lime glass. Cr thin film has used for various industrial fields such as lithography masks, encoder slits for precision stages, and nano-optics. Ultrashort pulse laser micromachining can be adopted to the fabrication and repair of micro-patterning of Cr thin films. Soda-lime glass has generally been used as an inexpensive substrate for biochips with micro-channels, transparent microstructures for micro-devices, etc. Through these phenomena, we discuss the fabrication feasibilities of ultrashort pulse micromachining and propose the optimal process conditions for ultrashort pulse machining

TABLE 1. Physical properties of Chromium

Atomic mass	51.99
Density at 20 °C	7.1 g/cm^3
Specific Heat at 25 °C	518 J/kg·K
Melting /Boiling Temperature	1857 °C / 2672 °C
Latent Heat of Fusion/Evaporation	260 J/g / 6580 J/g
Thermal Conductivity	94 W/m·K

processes.

II. EXPERIMENTAL CONFIGURATION

Fig. 1 shows the layout of an ultrashort pulse micromachining system using a Ti:sapphire regenerative amplifier (Coherent, RegA 9000). The amplifier generated 800 nm NIR output at a 100 kHz repetition rate. Few micro-joule pulses were emitted by this amplifier. Pulse characteristics were measured by an autocorrelator (Coherent) and a power meter (Molectron). The measured pulse width and the average power of the output beam were 220 fs and 0.5 W, respectively, at 100 kHz. A pulse generator (Agilent technologies) was used to control the pulse number from the laser source and was monitored by an oscilloscope to confirm the input signal. ND filters with various OD were used to attenuate the raw pulse energy from the amplifier. Microscope objective lenses (Olympus) of 20× (N.A.=0.4) and 100× (N.A.=0.8) were adopted to focus a laser beam with high irradiance on the samples. Theoretically calculated focused spot sizes of the microscope objective lenses were 2.5 μ(20X)m and 1.3 μ(100X)m. To move the sample precisely, a 3-axis translation stage was controlled by a PMAC controller within ± 1 μm accuracy. The motion pattern of the stage was programmable by PMAC software to move 3-dimensional shapes.

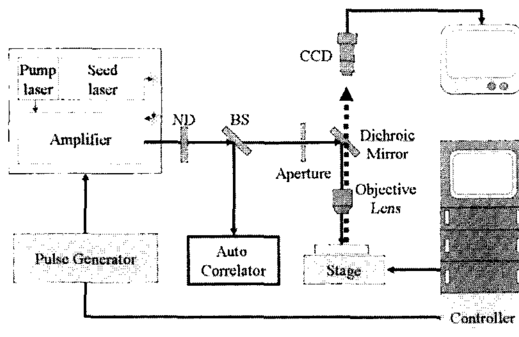

FIG. 1. Schematic diagram of femtosecond laser micromachining system

III. MICROSTRUCTURING OF CHROMIUM THIN FILM

In this section, results for the microstructuring of chromium thin film by using a fs laser are examined. The chromium thin film was coated on a glass substrate with 200 nm and 500 nm thickness, respectively. The physical properties of Cr are shown in Table 1. Fig. 2 shows ablated pit shapes by different ultrashort pulse energies with TEM_{00} beam mode and a schematic diagram of the pulse for each case. The diameter of the pit d can be described by Eq. (1) using a focused beam size d_0, irradiated pulse energy E, and the damage threshold of the sample E_{th}

$$d = d_0 \left(\ln \left(\frac{E}{E_{th}} \right) \right)^{1/2} \quad (1)$$

where d_0 is defined by Eq. (2)

$$d_0 = M^2 \frac{4}{\pi} \frac{f\lambda}{D} \quad (2)$$

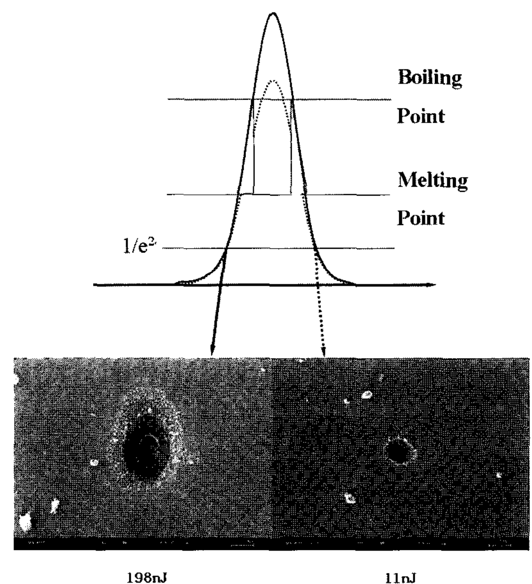

FIG. 2. Comparison of the morphology between high energy pulse and low energy pulse

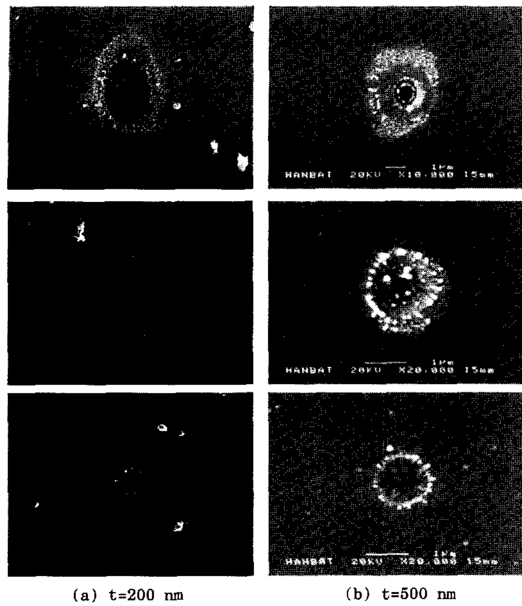

FIG. 3. SEM images of pits by a fs pulse of the indicated condition. Note the different magnifying power in these pictures. [(a) top = 198 nJ, middle = 39 nJ, bottom = 11 nJ / (b) top = 218 nJ, middle = 41 nJ, bottom = 12 nJ]

In Fig. 2, a pit formed by an 11 nJ pulse has smaller diameter than the calculated beam size because the effective area exceeding the damage threshold energy is only at the center of the whole beam. As the pulse energy increases, the pit size also increases up to d_0, and if excessive pulse energy irradiates, dross and recasting are generated around the ablated core. Two significant observations can be made from Fig. 3. First, the change of the pit size and shape increases according to the increase of pulse energy. Second, although the tendencies between different thicknesses of Cr film are similar with an increase in pit size according to irradiated pulse energy change, from a detailed perspective, it is different in proportion to the Cr film thickness. To understand these differences, dimensional parameters should be considered. The DOF (depth of focus) of the 100× microscope objective lens was calculated as $\pm$ 0.46 μm, and the thermal penetration depth of a metallic substrate is known to be of the order of a few 10^{-5} cm. It can be supposed that the critical depth lies between 200 nm and 500 nm to change the ablated morphology. In 200 nm Cr film, because the critical depth boundary would be in the glass substrate under the Cr film, discontinuous thermal conductivity would be generated. This seems to work as a barrier to block the transport of excessive energy. But in 500 nm thickness, due to the critical depth is smaller than 500 nm, energy transport would occur only in the chromium environment. In Fig. 4, the damage threshold can be assumed as 3 nJ. This figure shows

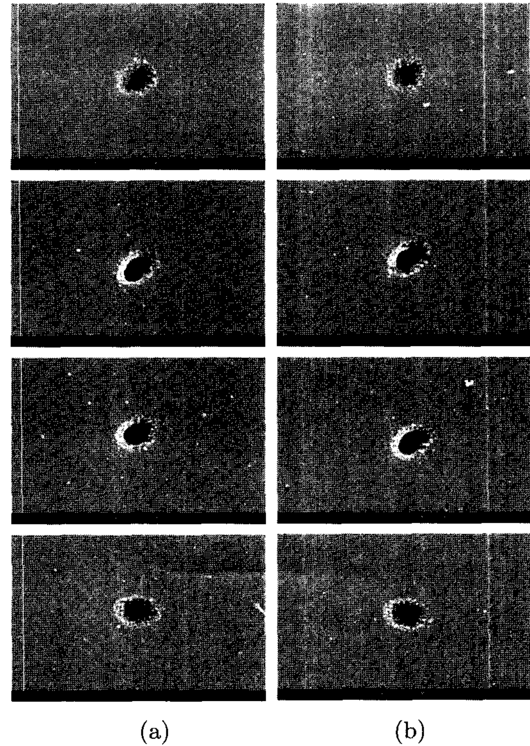

FIG. 4. SEM image of different focal position varying 1 μm from top to bottom and assist gas 5 pulses with each single pulse energy of 3.2 nJ at 100 kHz (a) He (b) No gases

that 5 pulses with 3.2 nJ of single pulse energy irradiated the Cr surface, as this was the smallest pulse energy that could change the Cr surface. Damaged features by pulse energy lower than 3.2 nJ could not be found. The pulse energy of 3.2 nJ can be described by irradiance as 1.1×10^{12} W/cm^2, and the reflectance of the Cr at 800 nm is known to be as large as 60%; thus the effective intensity would be less than half of 1.1×10^{12} W/cm^2. As shown in Figs. 4 (a) and (b), morphological differences could not be found according to assist gas change. However, some significant morphological differences were described in [8]; we are now studying the influence of assist gas. As a result of these experimental conclusions, grooving of the Cr film was performed with near damage threshold energy. Fig. 5 shows the groove shapes with various beam scanning speeds, 0.1 mm/sec, 1 mm/sec, and 10 mm/sec. In this experiment, unlike the case of the pitting process, it is assumed that an incubation effect affected the result [9]. Hence a smaller pulse energy than the damage threshold could ablate Cr. As the overlap ratio can be easily calculated between the slow moving case and the fast moving case at 100 kHz, in the case of slow moving of the stage with 0.1 mm/sec, the pulse energy would accumulate 100 times more than that at 10 mm/sec, and the incubation effect

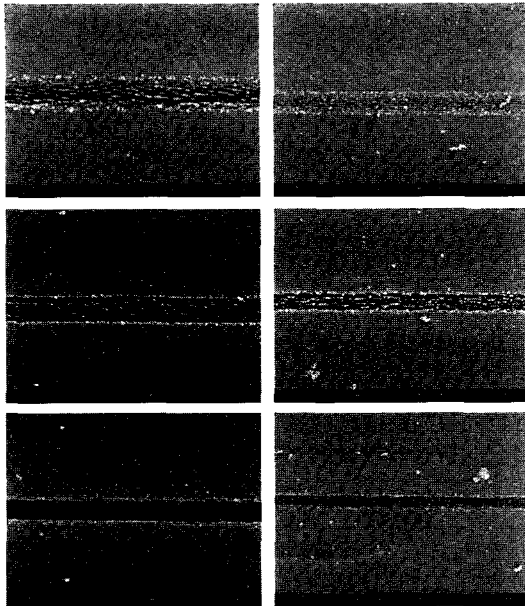

FIG. 5. SEM images of line ablation during moving sample with the speed of 0.1 mm/sec, 1 mm/sec and 10 mm/sec from the top at the energy of (a) 4.7 nJ (b) 1.6 nJ . Line width : (a) 1.37 μm, 1.2 μm, 1.0 μm (b) 1.0 μm, 0.75 μm, 0.62 μm

would become more dominant than for the fast moving at a high repetition rate such as 100 kHz. This clearly shows that excessive energy irradiation by slow moving of the sample seems to break the two-temperature conditions. Therefore, processing with near threshold pulse energy and overlap under 95% would be the optimal conditions for HAZ-free grooving of Cr thin film.

IV. MICROSTRUCTURING OF SODA-LIME GLASS

The physical properties and approximate composition of the soda-lime glass are shown in Tables 2 and 3, and a graph of the transmission is presented in Fig. 6. As generally known, glass is a wide band gap material and is transparent at UV to NIR. In addition, glass is hard to fabricate using a long pulse laser because of its brittle and weak nature in terms of thermal stress. But in the high intensity regime, nonlinear absorption is started by the multiphoton ionization effect [10] and photochemical ablation also commences. This is the key effect for glass micromachining using an ultrashort pulse. Fig. 7 shows a comparison of glass processing using a 800 *nm* NIR pulse with 220 fs duration and a 355 nm UV pulse with an order of ns duration ($\sim$ 40 ns). Wide HAZ is seen around the groove in Fig. 7 (b), but in Fig. 7 (a), HAZ is not found. This clearly shows that photochemical ablation is a dominant process in femtosecond pulse interaction while the photothermal effect is the leading mechanism in nanosecond or longer pulse duration regime. In Fig. 8, each ablation pattern with different pulse energy is shown. Pulse energy was varied at 600 nJ, 520 nJ, 460 nJ, and 90 nJ under the same moving speed of 80 mm/sec. These values of pulse energy could be described as intensities, such as 600 nJ to 2.2 $\times$ 10^{14} W/cm^2 and 90 nJ to 3.5 $\times$ 10^{13} W/cm^2, while the calculated beam size was 1.3 μm. Upon examination

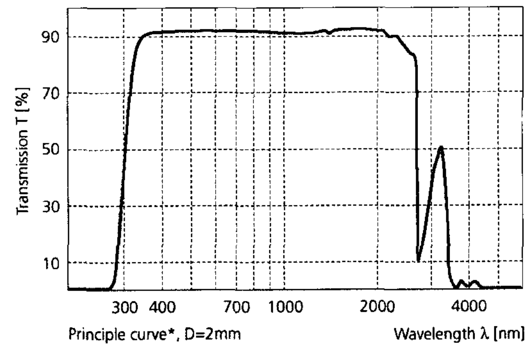

FIG. 6. Transmission curve of glass

TABLE 2. Physical properties of Soda-lime glass

Density	2470 kg/m^3
Tg	818K
Specific heat capacity	670 J/kg·K
Thermal Conductivity	0.95 W/m·K
Linear expansion coefficient at Room temp.	0.9 $\times$ 10^{-5}/K

TABLE 3. Approximate composition (% by wt) for soda-lime glass

SiO_2	Na_2O	CaO	MgO	Al_2O_3
72.6	15.2	4.6	3.6	1.7

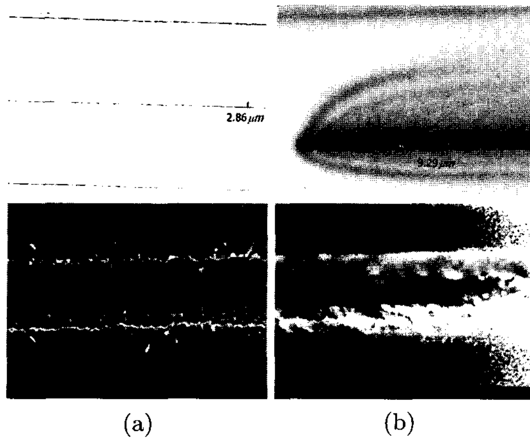

(a) (b)

FIG. 7. Phase contrast microscope images (top) and SEM images (bottom) of laser ablation of glass with 220 fs pulse at 800 nm (a) and 40 ns pulse at 355 nm (b). Note the different magnifying power in these pictures.

of Fig. 8 (d), it can be assumed that the damage threshold of the soda-lime glass is close to 3.5×10^{13} W/cm^2. Another important parameter in influencing laser machining quality is the beam scanning speed. The beam scanning speed determines the overlap ratio of successive beam spots. Fig. 9 shows SEM images of the ablated glass surface with various beam scanning speeds. The beam scanning speed was varied from 80 mm/s to 20 mm/s, and the overlap ratio was calculated by using the focused beam size and laser repetition rate. Because we used a 100× microscope objective lens and a 100 kHz amplifier, the overlap ratio was obtained from 29% to 85%. For good edge quality of the groove, slow scanning speed and a high overlap ratio would be suitable, as shown in Fig. 8 (d). We used this result to fabricate a micro channel with a 40 μm line width. The dimensions of the micro-channel were 40 μm in width and 25 μm in height. Changing the microscope objective lens to 20× (NA=0.4), the focused beam size was changed to 2.5 μm. Consequently the beam scanning speed was changed to 10 mm/s (96%) and 70 mm/s (72%). The lateral pitch of the lines inside the pattern of the micro-channel was 3 μm. This means that overlap did not exist between lateral lines, and only an incubation effect

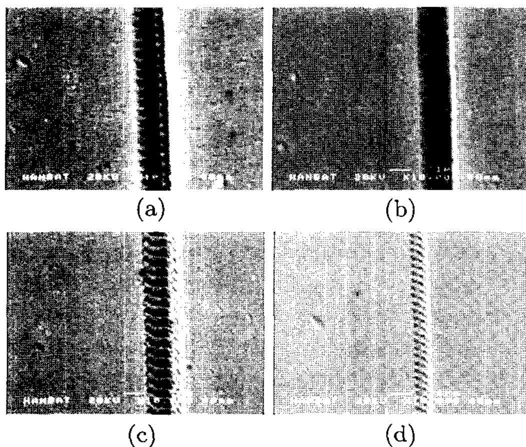

(a) (b)

(c) (d)

FIG. 8. SEM images of fs pulse ablation of glass with various pulse energy [(a) 600 nJ, (b) 520 nJ, (c) 460 nJ, (d) 90 nJ]

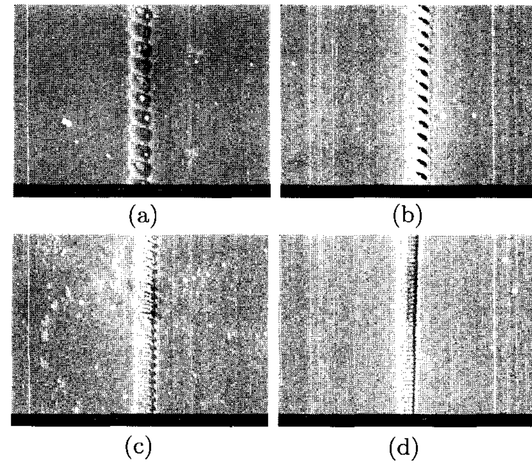

(a) (b)

(c) (d)

FIG. 9. SEM images of ablated glass surface with various beam scanning speed [(a) 80 mm/s, (b) 60mm /s, (c) 40 mm/s, (d) 20 mm/s]

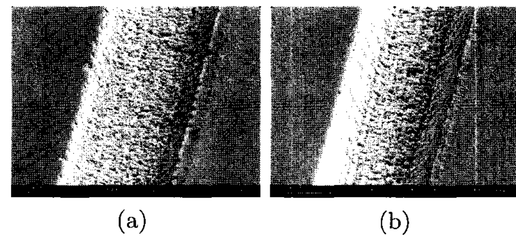

(a) (b)

FIG. 10. SEM images of a micro channel on glass surface [scanning speed - (a) 70 mm/s, (b) 10 mm/s]

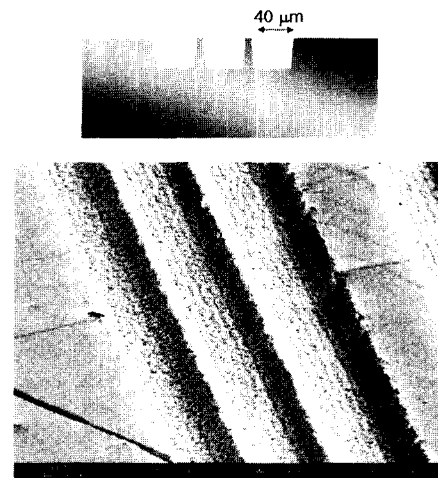

FIG. 11. SEM image of a micro channel array on glass surface and its side view drawing

would accumulate in the lateral direction. In Fig. 10, the edge quality of the micro-channel with 10 mm/s (b) was shown to be better than that for 70 mm/s (a). In Fig. 11, a micro-channel array with the same dimensions as that in Fig. 10 is shown. This could be used for micro-optical devices, lab on a chip, or other micro-fluidic devices. Because we used a 100 kHz regenerative amplifier, 100 times fast moving with high overlap ratio over 90% is possible. This is an advantage of a high repetition rate source for high throughput with good quality.

V. CONCLUSION

We drew various machining conditions in carrying out micromachining for Cr thin film and soda-lime glass by using ultrashort pulse. Although there are physically different properties between metal and transparent dielectric materials, we have confirmed that sub-micrometer structures with minimized HAZ can be obtained by using ultrashort pulse, and there are few differences in basic machining shapes. The damage thresholds of Cr and soda-lime glass were obtained experimentally, and these were important to estimate optimal conditions. As our demonstrations illustrated, we obtained machining shapes of good quality. It is important to control scanning speed to maintain a 95% overlap ratio because exceedingly overlapped machining can devaluate quality by an incubation effect. Our results demonstrate that ultrashort pulse laser micromachining is suitable to fabricate microstructures. One of the bottlenecks of applying femtosecond lasers to the industrial mass-production level has been the poor throughput owing to its low repetition rate and low etch rate. But a high repetition rate source with moderate pulse energy to fabricate industrial materials such as metals, ceramics, and glass could sufficiently increase the throughput to apply a femtosecond laser machining system to mass-production industries.

*Corresponding author : jychoi@kimm.re.kr.

REFERENCES

[1] D. Strickland and G. Mourou, "Compression of amplified chirped optical pulses," *Opt. Comm.*, vol. 56, pp. 219-222, 1985.

[2] T. Q. Qiu and C. L. Tien, "Heat transfer mechanisms during short-pulse laser heating of metals," *J. of Heat Transfer,* vol. 115, pp. 835-841, 1993.

[3] S. Valette, R. Le Harzie, E. Audouard, N. Hout, and R. Fortunier, "Modeling thermal effects produced by nanosecond and femtosecond laser pulses applied to metals," in *ICALEO Proc. '02*, 2002.

[4] C. B. Schaffer and E. Mazur, "Micromachining using ultrashort pulses from a laser oscillator," *Optics and Photonics news*, vol. April, pp. 20-24, 2001.

[5] B. N. Chichkov, F. Korte, J. Koch, and S. Nolte, "Femtosecond laser ablation and nanostructuring," *High Power Laser Ablation IV, Proc. SPIE,* vol. 4760, pp. 19-24, 2002.

[6] S Ameer-Beg, W. Perrie, S. Rathbone, J. Wright, W. Weaver, and H. Champoux, "Femtosecond laser micromachining of materials," *Applied Surface Science*, vol. 127-129, pp. 875-880, 1998.

[7] S. Nolte, C. Momma, G. Kamlage, A. Ostendorf, C. Fallnich, F. von Alvensleben, and H. Welling, "Polarization effects in ultrashort-pulse laser drilling," *Appl. Phys. A*, vol. 68, pp. 563-567, 1998.

[8] L. A. Walker II, R. L. Maynard, and W. Clark, "Atmospheric affects on ultrashort-pulsed materials processing," in *ICALEO Proc. '02*, 2002.

[9] A. Rosenfeld, M. Lorenz, R. Stoian, and D. Ashkenasi, "Ultrashort-laser-pulse damage threshold of transparent materials and the role of incubation," *Appl. Phys. A,* vol. 69, pp. 373-276, 1999.

[10] C. B. Schaffer, *Interaction of femtosecond laser pulses with transparent materials*, (Ph.D. thesis, Harvard University, USA, 2001).